We are IntechOpen, the world's leading publisher of Open Access books Built by scientists, for scientists

6,900
Open access books available

185,000
International authors and editors

200M
Downloads

154
Countries delivered to

Our authors are among the

TOP 1%
most cited scientists

12.2%
Contributors from top 500 universities

CLARIVATE ANALYTICS
BOOK CITATION INDEX
INDEXED

WEB OF SCIENCE™

Selection of our books indexed in the Book Citation Index
in Web of Science™ Core Collection (BKCI)

Interested in publishing with us?
Contact book.department@intechopen.com

Implementation of Induction Motor Drive Control Schemes in MATLAB/Simulink/dSPACE Environment for Educational Purpose

Christophe Versèle, Olivier Deblecker and Jacques Lobry
Electrical Engineering Department, University of Mons
Belgium

1. Introduction

Squirrel-cage induction motors (IM) are the workhorse of industries for variable speed applications in a wide power range that covers from fractional watt to megawatts. However, the torque and speed control of these motors is difficult because of their nonlinear and complex structure. In the past five decades, a lot of advanced control schemes for IM drive appeared. First, in the 1960's, the principle of speed control was based on an IM model considered just for steady state. Therefore, the so-called "scalar control methods" cannot achieve best performance during transients, which is their major drawback. Afterwards, in the 1970's, different control schemes were developed based on a dynamic model of the IM. Among these control strategies, the vector control which is included in the so-called field oriented control (FOC) methods can be mentioned. The principle of vector control is to control independently the two Park components of the motor current, responsible for producing the torque and flux respectively. In that way, the IM drive operates like a separately excited dc motor drive (where the torque and the flux are controlled by two independent orthogonal variables: the armature and field currents, respectively). Since the 1980's, many researchers have worked on improvements of the FOC and vector control which have become the industry's standard for IM drives. Moreover, these researches led to new control strategies such as direct self control (DSC) or direct torque control (DTC). The principle of DTC is to control directly the stator flux and torque of the IM by applying the appropriate stator voltage space vector.

With vector control, FOC, DSC and DTC, the major drawback of the scalar control is overcome because these control schemes are based on a model of the IM which is considered valid for transient conditions (Santisteban & Stephan, 2001). Both DTC and DSC possess high torque dynamics compared to vector control and FOC (Böcker & Mathapati, 2007). However, these two first control techniques have the drawbacks of variable switching frequency and higher torque ripple. The use of space vector pulse-width-modulation (SV-PWM) in conjunction with DTC (called, in this chapter, DTC-space vector modulation or DTC-SVM) has been proposed as a solution to overcome these drawbacks (Rodriguez et al., 2004), but sticking to the fundamental concept of DTC.

The objective of this chapter is neither to do an overview of all IM control methods, as is done, e.g., in (Böcker & Mathapati, 2007; Santisteban & Stephan, 2001), nor to try to

ameliorate them. Its aim is to present a powerful tool to help students to understand some IM control schemes, namely the scalar control method, the vector control and the DTC-SVM, of a voltage-fed inverter IM drive using a dSPACE platform and Matlab/Simulink environment. First, they determine the IM parameters using a procedure based on the implemented vector control scheme. The accuracy of these measurements is very important because the considered control methods need precise information about the motor parameters (Böcker & Mathapati, 2007). Then, after concluding off-line simulations, they perform some experiments in speed regulation and speed tracking.

The remainder of this chapter is organized as follows. First, the experimental system is presented. Then the IM models used therein are described and the determination of the IM parameters as well as the implementation of the control methods are exposed. Finally, typical results are presented and the educational experience is discussed.

2. Experimental system

The experimental system consists of three essentials parts: (1) the power driver, (2) the control system and (3) the transducers. Fig. 1 shows a synoptic scheme of the experimental platform.

The power driver consists of a voltage-fed inverter and two machines: one squirrel-type IM of rated power 5.5 kW and a dc-machine with a separately excited field winding of rated power 14.6 kW. These machines are mechanically coupled and the dc-machine is used as the load of the IM.
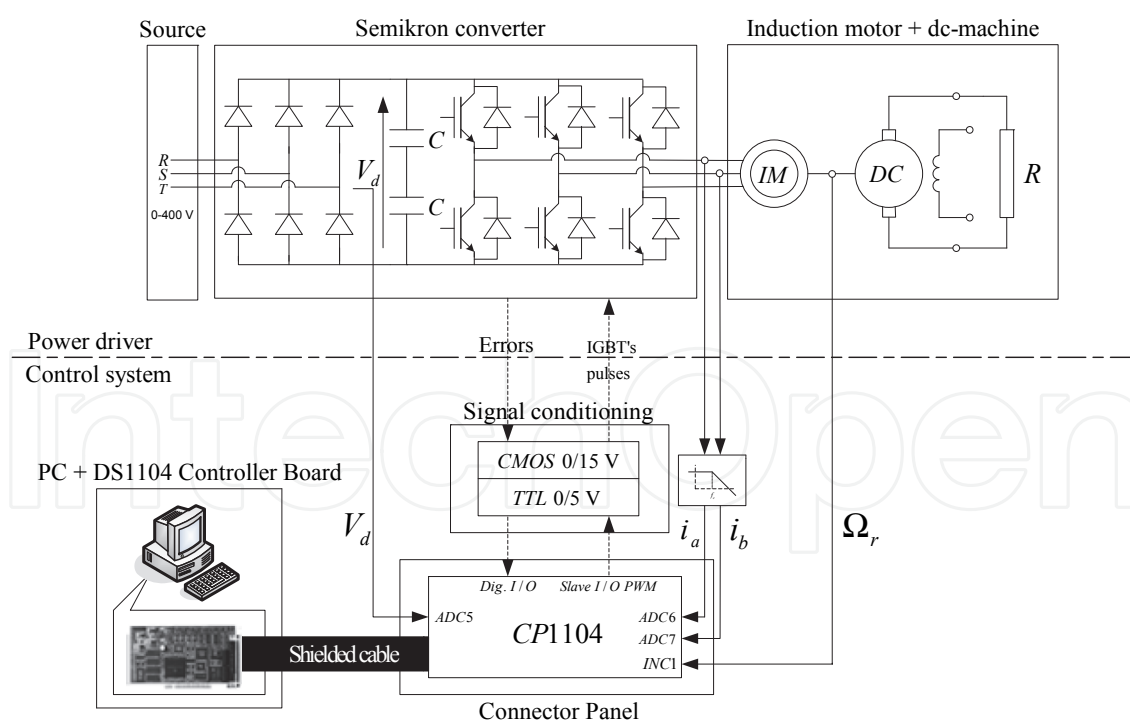

Fig. 1. Synoptic scheme of the experimental platform

The control system is based on the DS1104 Controller Board by dSPACE plugged in a computer. Its development software operates under Matlab/Simulink environment (Bojoi et al., 2002) and is divided into two main components: Real Time Interface (RTI) which is the

implementation software and ControlDesk which is the experimentation software. RTI is a Simulink toolbox which provides blocks to configure models (Bojoi et al., 2002). These blocks allow the users to access to the dSPACE hardware. ControlDesk allows, as for it, the users to control and monitor the real-time operation by using a lot of virtual instruments and building a control window.

When using dSPACE, the several steps required to implement a control system on the DS1104 Controller Board are described below. The first step consists in modeling the control system with Simulink and configuring the I/O connections of the Connector Panel thanks to the RTI toolbox. After that, the Real-Time Workshop (RTW) toolbox, using RTI, automatically generates the C-code for the board. Once the execution code has been generated, the dSPACE hardware can perform a real-time experiment which can be controlled from a PC with ControlDesk. ControlDesk can be used to monitor the simulation progress, adjust parameters online, capture data (in a format compatible with Matlab) and communicate easily with the upper computer real-time (Luo et al., 2008). Fig. 2 presents the connections between Matlab and dSPACE.

The experimental system contains several current and voltage LEM transducers as well as a speed sensor. Moreover, the measured currents must be filtered in order to avoid aliasing when they will be converted into digital signals. Therefore, an anti-aliasing filter is added to each current transducer. The cut-off frequency of this filter is estimated at 500 Hz (an order of magnitude above the rated frequency of 50 Hz).
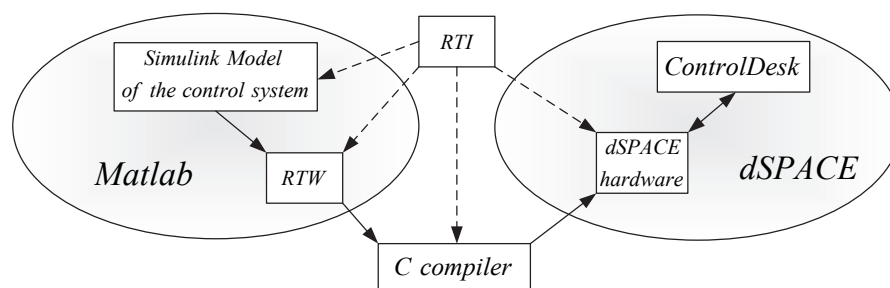

Fig. 2. Connections between Matlab and dSPACE (Mäki et al., 2005)

3. IM modeling

A simple per phase equivalent circuit model of an IM is interesting for the analysis and the performance prediction at steady-state condition. Such a model is therefore used in this chapter for scalar control. In the two other considered control schemes, namely vector control and DTC-SVM, the transient behaviour of the IM has to be taken into account. So, the dynamic d-q model of the IM based on the Park's transformation is considered. These two well-known types of IM models are available in literature (see, e.g., (Bose, 2002; Mohan, 2001)) and are briefly recalled in this section.

3.1 Steady-state model of IM

The considered steady-state IM model, based on complex phasors, is shown in Fig. 3(a). This model is an equivalent circuit with respect to the stator and can easily be established from the short-circuited transformer-equivalent circuit (Bose, 2002).

The synchronously rotating air gap flux wave generates an electromotive force E_s which differs from the stator terminal voltage V_s by the drop voltage in stator resistance R_s and

stator leakage inductance l_s. The stator current I_s consists of the magnetizing current I_m and the rotor current I_r (referred to the stator in Fig. 3(a)) which is given by (Bose, 2002):

$$I_r = \frac{E_s}{\dfrac{R_r}{s} + j \cdot 2 \cdot \pi \cdot f \cdot l_r} .$$ (1)

where R_r is the rotor resistance (referred to the stator), l_r is the rotor leakage inductance (referred to the stator), s is the slip and f is the stator supply frequency. Finally, in Fig. 3(a), L_m is the magnetizing inductance and R_m is the equivalent resistance for the core loss.

The equivalent circuit of Fig. 3(a) can be further simplified as shown in Fig. 3(b) where the resistance R_m has been dropped and the inductance l_s has been shifted to the other side of the inductance L_m.
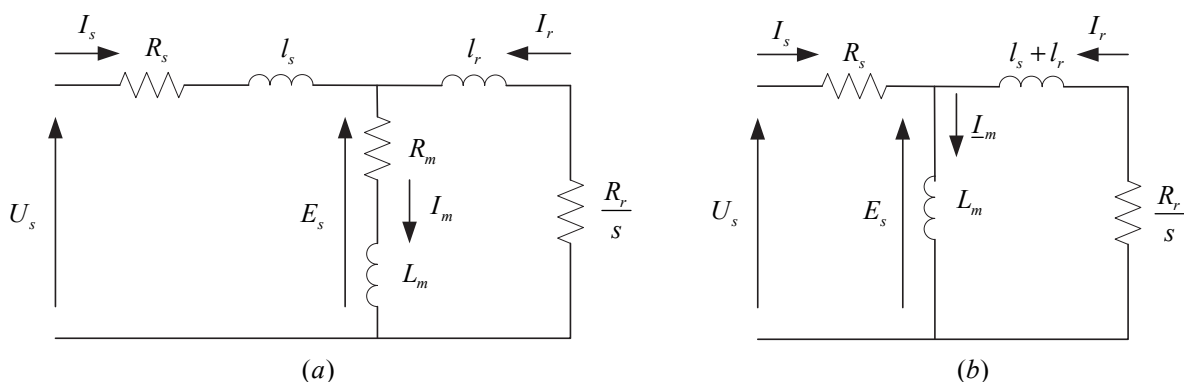
Fig. 3. (a) Equivalent circuit with respect to the stator and (b) Approximate per phase equivalent circuit

This approximation is easily justified as the value of the magnetizing inductance is, at least, one order of magnitude greater than the value of the stator leakage inductance. Moreover, the performance prediction by the approximate equivalent circuit typically varies within 5% from that of the actual machine (Bose, 2002).

Based on the equivalent circuit of Fig. 3(b), it can be demonstrated (see, e.g., (Bose, 2002)) the following expression of the electromagnetic torque:

$$T_e = 3 \cdot P \cdot R_r \cdot \frac{(s \cdot \omega) \cdot \psi^2}{R_r^2 + (s \cdot \omega)^2 \cdot (l_s + l_r)^2}$$ (2)

where P is the number of poles pairs and ψ is the stator flux. It should also be emphasized that for small slip values, (2) can be rewritten as:

$$T_e = \frac{3 \cdot P \cdot \psi^2}{R_r} \cdot (s \cdot \omega) = K_T \cdot (s \cdot \omega)$$ (3)

where K_T is a constant if the flux is kept constant.

Finally, for steady-state operation of IM, the rotational speed Ω_r can be calculated by:

$$\Omega_r = (1 - s) \cdot \frac{2 \cdot \pi \cdot f}{P} .$$ (4)

3.2 Dynamic model of IM

Applying the usual space vector transformation to a three-phase system, it is possible to obtain the following set of equations, based on space vectors, that describes the IM dynamic behavior in a stator fixed coordinate system (Rodrigez et al., 2004):

$$\mathbf{v_s} = R_s \cdot \mathbf{i_s} + \frac{d\mathbf{\psi_s}}{dt} + j \cdot \omega_1 \cdot \mathbf{\psi_s} \tag{5}$$

$$\mathbf{v_r} = 0 = R_r \cdot \mathbf{i_r} + \frac{d\mathbf{\psi_r}}{dt} + j \cdot \left(\omega_1 - P \cdot \Omega_r\right) \cdot \mathbf{\psi_r} \tag{6}$$

$$\mathbf{\psi_s} = l_s \cdot \mathbf{i_s} + L_m \cdot \left(\mathbf{i_s} + \mathbf{i_r}\right) \tag{7}$$

$$\mathbf{\psi_r} = l_r \cdot \mathbf{i_r} + L_m \cdot \left(\mathbf{i_s} + \mathbf{i_r}\right) \tag{8}$$

where ω_1 is the rotational speed of the d-q reference frame, $\mathbf{v_s}$ and $\mathbf{v_r}$ are respectively the stator and rotor voltages, $\mathbf{i_s}$ and $\mathbf{i_r}$ are respectively the stator and rotor currents and $\mathbf{\psi_s}$ and $\mathbf{\psi_r}$ are respectively the stator and rotor fluxes.

The electromagnetic torque developed by the IM can be expressed in terms of flux and current space vector by several analog expressions. In this chapter, two of them are useful:

$$T_e = \frac{3}{2} \cdot P \cdot \frac{L_m}{L_r} \cdot \left[\mathbf{\psi_r} \times \mathbf{i_s}\right] \tag{9}$$

and

$$T_e = \frac{3}{2} \cdot P \cdot \frac{L_m}{\sigma \cdot L_s \cdot L_r} \cdot \left[\mathbf{\psi_s} \times \mathbf{\psi_r}\right] \tag{10}$$

where L_s ($L_s = L_m + l_s$) and L_r ($L_r = L_m + l_r$) are respectively the stator and rotor inductances and σ is the leakage factor of the IM defined as:

$$\sigma = 1 - \frac{L_m^2}{L_s \cdot L_r} . \tag{11}$$

The speed Ω_r cannot normally be treated as a constant (Bose, 2002). It can be related to torque using the IM drive mechanical equation which is:

$$T_e = J \cdot \frac{d\Omega_r}{dt} + B \cdot \Omega_r \tag{12}$$

where J and B denote respectively the total inertia and total damping of the IM coupled to the dc-machine.

Finally, the dynamic model of the IM is shown in Fig. 4 in its complex form for compact representation.

4. Control schemes

4.1 Scalar control

Scalar control is due to magnitude variation of the control variables only and disregards the coupling effect in the machine (Bose, 2002). Although having inferior performances than the
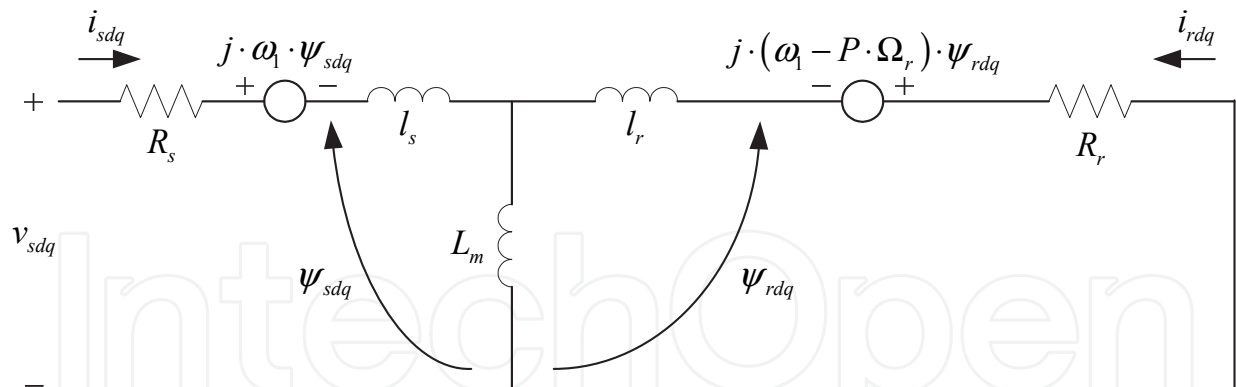
Fig. 4. Dynamic model of IM

two other considered control schemes, it is considered in this chapter because it has been widely used in industry and it is easy to implement. So, this is a good basis for the study of IM drive. Among the several scalar control techniques, the open loop Volts/Hz control of IM, which is the most popular method of speed control of a voltage-fed inverter IM, is used. For adjustable speed applications, frequency control appears to be natural considering (4). However, the stator voltage is required to be proportional to frequency so that the flux:

$$\psi = \frac{U_s}{2 \cdot \pi \cdot f} \tag{13}$$

remains constant (normally equal to its rated value), neglecting the stator resistance voltage drop. Indeed, if an attempt is made to reduce the frequency at the rated stator voltage, the flux will tend to saturate, causing excessive stator current and distortion of the flux waveforms (Bose, 2002). Therefore, in the region below the base frequency f_b (which can be different from the rated frequency), a reduction of the frequency should be accompanied by the proportional reduction of the stator voltage in order to maintain the flux to its rated value. Fig. 5 shows the torque-speed curves. It can be shown in this figure that in the region below the base frequency, the torque-speed curves are identical to each other and that the maximum torque T_{em} (which can be deduced from (2)) is preserved regardless of the frequency, except in the low-frequency region where the stator resistance voltage drop must be compensated by an additional boost voltage U_{boost} in order to restore the T_{em} value (as shown in Fig. 5).

Once the frequency increases beyond the base frequency, the stator voltage is kept constant and, therefore, the flux decreases. As shown in Fig. 5, in this flux-weakening region, the torque-speed curves differ from the previous ones and the developed torque decreases. An advantage of the flux-weakening mode of operation is that it permits to increase the speed range of the IM.

Fig. 6 shows the block diagram of the Volts/Hz speed control method. The frequency f^*, which is approximately equal to the speed neglecting the slip, is the primary control variable. The secondary control variable is the stator voltage U_s^* which is directly generated from the frequency command using the gain factor G so that the flux remains constant or a flux-weakening mode of operation is achieved. Moreover, at low-frequencies, corresponding to a low rotational speed of the IM, the boost voltage is added in order to have the maximum torque available at zero speed. Note that the effect of this boost voltage

becomes negligible when the frequency grows. Finally, the f^* command signal is integrated to generate the angle signal θ^* which in combination with $U_s{}^*$ produce the sinusoidal voltages.
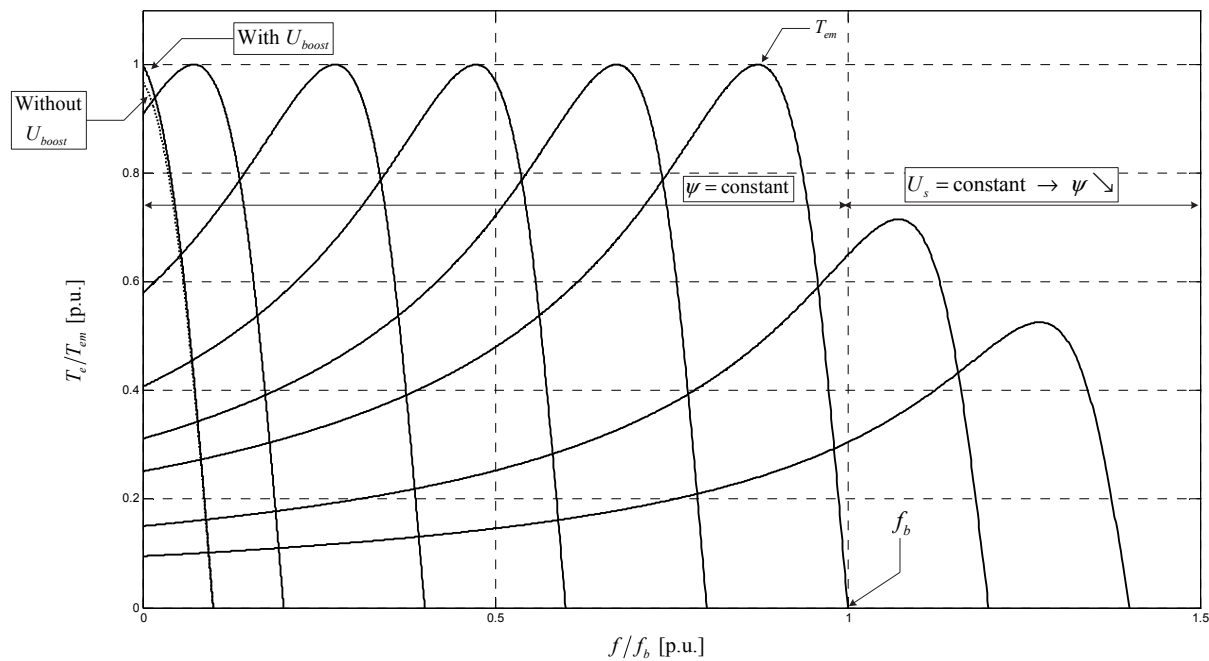

Fig. 5. Torque-speed curves at constant Volts/Hz region and in flux-weakening region

Note that an improvement of the open-loop Volts/Hz control is the close-loop speed control by slip regulation (see, e.g., (Bose, 2002)).
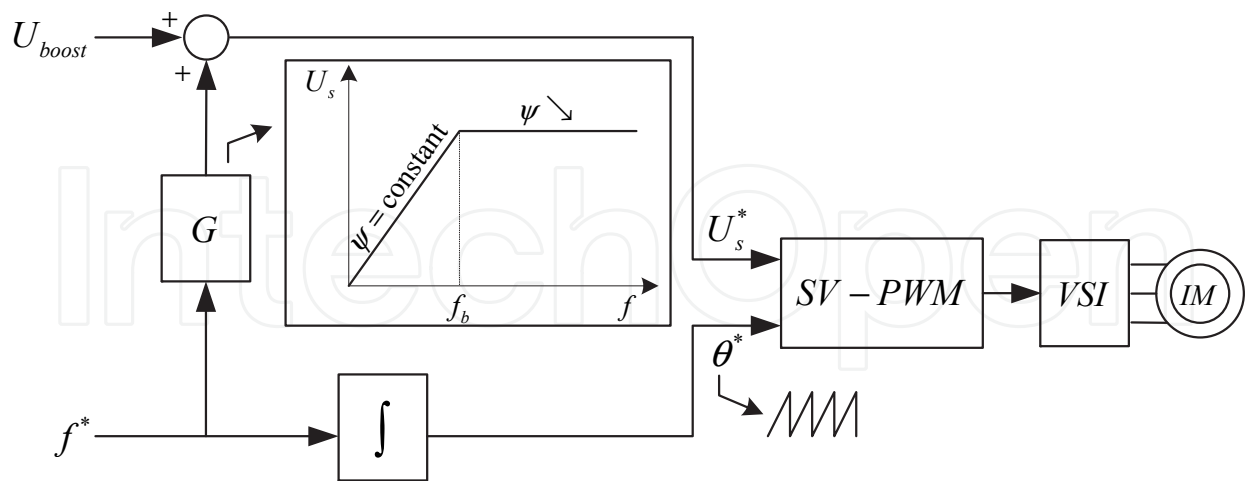

Fig. 6. Open-loop Volts/Hz control of IM

4.2 Vector control

The objective of vector control of IM is to allow an IM to be controlled just like a separately excited dc motor drive (where the torque and the flux are controlled by two independent orthogonal variables: the armature and field currents, respectively). This is achieved by a

proper choice of the so-called Park's rotating frame (*d-q* axes) in which the space vector equations (5)-(8) are separated into *d-q* ones.

In the *d-q* frame, (9) can be rewritten:

$$T_e = \frac{3}{2} \cdot P \cdot \frac{L_m}{L_r} \cdot \left(\psi_{rd} \cdot i_{sq} - \psi_{rq} \cdot i_{sd} \right) \tag{14}$$

where ψ_{rd} and ψ_{rq} are the rotor fluxes and i_{sd} and i_{sq} are the stator current in the dq-axes.

In this chapter, a direct vector control strategy in which the *d-q* frame rotates along with the rotor flux (which is maintained at its rated value) is considered. The *d*-axis is aligned with the direction of the rotor flux. Therefore, the *q*-axis component of the rotor flux is null and the expression of the electromagnetic torque simplifies as follows:

$$T_e = \frac{3}{2} \cdot P \cdot \frac{L_m^2}{L_r} \cdot i_{mr} \cdot i_{sq} \tag{15}$$

where i_{mr} is the rotor magnetizing current defined by:

$$\psi_{rd} = L_m \cdot i_{mr} . \tag{16}$$

Using (6) and (7) projected in the *d-q* frame as well as (16), the rotor magnetizing current can be expressed in terms of the *d*-axis stator current as follows:

$$i_{mr} + T_r \cdot \frac{di_{mr}}{dt} = i_{sd} \tag{17}$$

where T_r ($T_r = L_r / R_r$) is the rotor time constant.

From (15) and (17), one can conclude that the *d*-axis stator current (i_{sd}) is controlled to maintain the flux at its rated value whereas the *q*-axis stator current (i_{sq}) is varied to achieve the desired electromagnetic torque. Therefore, the IM can be controlled just like a separately excited dc motor drive because the *d*- and *q*-axes are orthogonal.

Note that, at each sample time, direct vector control of the IM requires to know the module and phase of the rotor flux. Therefore, a flux observer is used. Its task is to provide an estimate of the rotor flux (or rotor magnetizing current) in module and phase using the measured stator currents (converted in *d-q* components) and speed.

Once a flux estimate is available, the torque can easily be computed using (15). The flux observer implemented in the Simulink/dSPACE environment is shown in Fig. 7. As can be seen in this figure, the phase μ of the rotor magnetizing current is obtained by integrating the angular speed ω_1 of the *d-q* axes in the fixed stator reference frame.

In vector control, the IM is fed by a Voltage Supply Inverter (VSI) and a SV-PWM is used to produce the instantaneous generation of the commanded stator voltages. The required *d*-axis and *q*-axis stator voltages (v_{sd} and v_{sq}) that the VSI must supply to the IM, in order to make the stator currents (i_{sd} and i_{sq}) equal to their reference values are expressed as follows:

$$v_{sd} = R_s \cdot \left[i_{sd} + T_s \cdot \left(\sigma \cdot \frac{di_{sd}}{dt} + (1 - \sigma) \cdot \frac{di_{mr}}{dt} - \sigma \cdot \omega_1 \cdot i_{sq} \right) \right] \tag{18}$$

$$v_{sq} = R_s \cdot \left[i_{sq} + T_s \cdot \left(\sigma \cdot \frac{di_{sq}}{dt} + (1 - \sigma) \cdot \omega_1 \cdot i_{mr} - \sigma \cdot \omega_1 \cdot i_{sd} \right) \right] \tag{19}$$
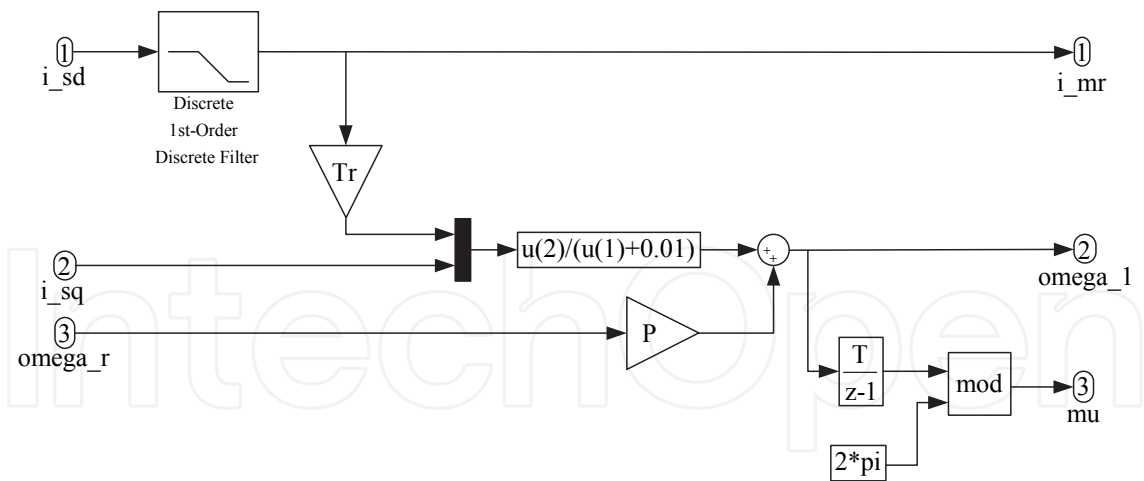
Fig. 7. Flux observer implemented in Matlab/Simulink/dSPACE environment

where T_s ($T_s = L_s/R_s$) is the stator time constant.

In the d-axis (respectively q-axis) voltage equation, only the first two terms of the right-hand side are due to the d-component (respectively q-component) of the stator current, i_{sd} (respectively i_{sq}). The other terms, due to i_{mr} and i_{sq} (respectively i_{mr} and i_{sd}) can be considered as disturbances (Mohan, 2001). So, (18) and (19) can simply be rewritten as:

$$v'_{sd} = R_s \cdot \left[i_{sd} + \sigma \cdot T_s \cdot \frac{di_{sd}}{dt} \right] \qquad (20)$$

$$v'_{sq} = R_s \cdot \left[i_{sq} + \sigma \cdot T_s \cdot \frac{di_{sq}}{dt} \right]. \qquad (21)$$

Note that, in order to account for the terms considered as disturbances, a "decoupling compensator" block is incorporated in the vector control scheme.

The vector control scheme is shown in Fig. 8 with the reference values indicated by '*'. This control scheme matches to a direct vector control strategy in which the rotor flux is assigned to a reference value (its rated value as mentioned above).

The d-axis reference current, i^*_{sd}, controls the rotor flux (through the rotor magnetizing current) whereas the q-axis current, i^*_{sq}, controls the electromagnetic torque developed by the IM. The reference currents in the d- and q-axes are generated by a flux control loop and a speed control loop, respectively. The d-axis and q-axis voltages, v'_{sd} and v'_{sq}, are calculated from the given reference currents and using (20) and (21). To obtain these command signals, two PI controllers (in two inner current loops) are employed and it is assumed that the compensation is perfect. The terms considered as disturbances are then added to the voltages v'_{sd} and v'_{sq} in the "decoupling compensator" block. Hence, the d-axis and q-axis reference voltages, v_{sd} and v_{sq}, are obtained. Finally, these reference voltages are converted into the reference three-phase voltages v_a, v_b and v_c and supplied (in an approximate fashion over the switching period) by the VSI using the SV-PWM technique. Note that the four controllers are tuned by the pole-zero compensation technique.

4.3 DTC-SVM

Direct torque control of IM consists in closed-loop control of the stator flux and torque using estimators of these two quantities (Trzynadlowski et al., 1999).
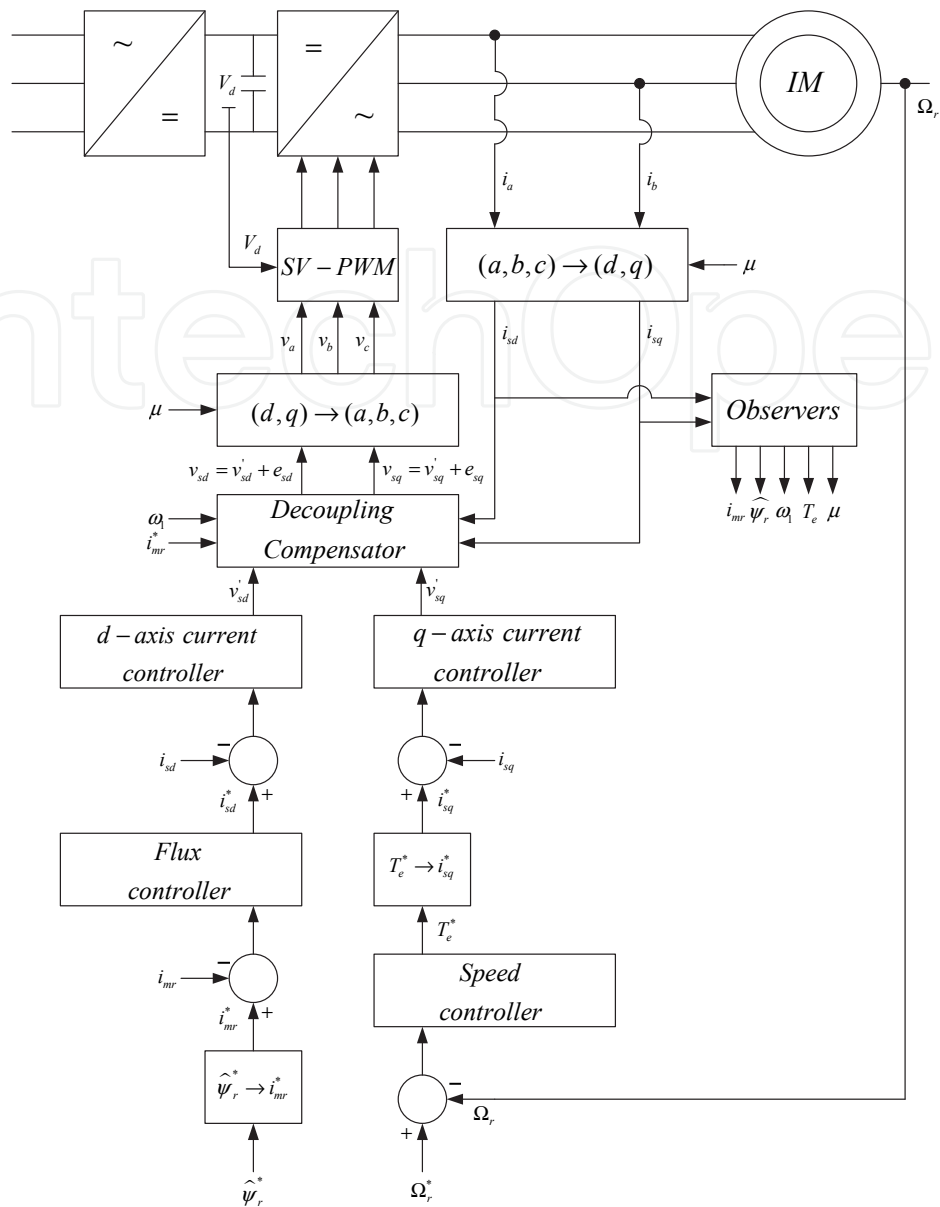
Fig. 8. Vector control scheme

From the IM dynamic model (5)-(8), the following equation can be obtained:

$$\frac{d\mathbf{\psi_r}}{dt} + \left(\frac{1}{\sigma \cdot T_r} - j \cdot P \cdot \Omega_r\right) \cdot \mathbf{\psi_r} = \frac{L_m}{\sigma \cdot T_r \cdot L_s} \cdot \mathbf{\psi_s} \tag{22}$$

which shows that the relationship between the stator and rotor fluxes is of low-pass filter type with time constant $\sigma \cdot T_r$ (Casadei et al., 2005). Otherwise stated, the rotor flux will follow a change in the stator flux with some delay (typically of the order of a few tenths of ms).

Equation (10) can also be rewritten as follows:

$$T_e = \frac{3}{2} \cdot P \cdot \frac{L_m}{\sigma \cdot L_s \cdot L_r} \cdot \psi_s \cdot \psi_r \cdot \sin\delta \tag{23}$$

where δ is the angle between the stator and rotor fluxes.

Based on the previous expression, it is clear that it is possible to achieve machine torque control directly by actuating over the angle δ (Rodriguez et al., 2004). DTC is founded on this consideration.

Due to slow rotor flux dynamic, the easiest way to change δ is to force a variation in the stator flux. Neglecting the effect of the voltage drop across the stator resistance, the stator flux vector in (5) is the time integral of the stator voltage vector. Hence, for sampling time Δt sufficiently small, (5) can be approximated as (Rodriguez et al., 2004):

$$\Delta \boldsymbol{\psi}_s \approx \Delta t \cdot \mathbf{v}_s \tag{24}$$

which means that the stator flux can be changed in accordance with the stator voltage vector supplied to the IM.

In the conventional DTC drive, the flux and torque magnitude errors are applied to hysteresis comparators. The outputs of these comparators are used to select the appropriate stator voltage vector to apply to the IM by means of a pre-designed look-up table. This scheme is simple and robust but it has certain drawbacks such as variable switching frequency and large current and torque ripples. Note that these ripples are imposed by the hysteresis-band width chosen for the hysteresis comparators.

In this chapter, the conventional DTC scheme is not considered but the so-called DTC-SVM scheme, which is discussed in details in (Rodriguez et al., 2004) and briefly presented below, is used. The objective of this alternative DTC scheme is to select the exact stator voltage vector that changes the stator flux vector according to the δ angle reference (calculated from the torque reference), while keeping the stator flux magnitude constant. SV-PWM technique is used to apply the required stator voltage vector to the IM.

The DTC-SVM scheme is shown in Fig. 9 with the reference values once again indicated by '*'. In this scheme, the torque reference is obtained from the speed reference thanks to the same speed controller as the one used in vector control. The error between the estimated torque and its reference value is processed through a PI controller to calculate the δ angle. From this angle, as well as the module of the stator flux (imposed at its rated value) and the estimated phase of the rotor flux, the block "Flux calculator" gives the stator flux reference according to:

$$\boldsymbol{\psi}_s^* = \left|\boldsymbol{\psi}_s\right|^* \cdot \cos\left(\delta + \angle\boldsymbol{\psi}_r\right) + j \cdot \left|\boldsymbol{\psi}_s\right|^* \cdot \sin\left(\delta + \angle\boldsymbol{\psi}_r\right) \tag{25}$$

The error between this reference quantity and the estimated stator flux is then divided by Δt, according to (24), in order to obtain the reference stator voltage vector. An approximation of that vector (over the switching period) is then supplied to the IM by the VSI using SV-PWM.

As explained above, the stator and rotor fluxes as well as the torque must be estimated. This is realized by the block "Torque and flux estimators". The rotor flux estimator is based on the IM model and implemented as follows:

$$\boldsymbol{\psi}_r = \frac{1}{T_r} \int \left(L_m \cdot \mathbf{i}_s - \left(1 - j \cdot T_r \cdot P \cdot \Omega_r\right) \cdot \boldsymbol{\psi}_r\right) \cdot dt . \tag{26}$$

The stator flux is, as for it, derived from:

$$\boldsymbol{\psi}_s = \sigma \cdot L_s \cdot i_s + \frac{L_r}{L_m} \cdot \boldsymbol{\psi}_r . \tag{27}$$

Fig. 9. DTC-SVM scheme

Once the stator and rotor fluxes estimates have been made available, the torque can be easily computed using (23). The observers of the stator and rotor fluxes implemented in the Matlab/Simulink/dSPACE environment are shown in Fig. 10.

The speed controller is tuned by the pole-zero compensation technique whereas the PI, that generates the δ angle reference, is tuned through a method based on the relay feedback test (Padhy & Majhi, 2006).

Fig. 10. Fluxes observers implemented in Matlab/Simulink/dSPACE environment

5. Determination of IM parameters

As it is well known, the control methods of IM require an accurate determination of machine parameters. Typically, five parameters need to be determined:

- R_s, R_r – the stator and rotor resistances;
- l_s, l_r – the stator and rotor leakage inductances;
- L_m – the magnetizing inductance.

In this chapter, the above parameters are determined both by a procedure founded on the vector control scheme (discussed in details in (Bose, 2002; Khambadkon et al., 1991)) and by a conventional method (no-load and blocked rotor tests).

The method based on the vector control scheme is divided into eight steps. Initially, the name plate machine parameters are stored into the computer's memory. Precisely, the method needs to know the rated stator voltage and current, the rated frequency and the number of poles pairs of the IM.

In a second step, the stator resistance is determined by a test at dc level. Next, the stator transient time constant is measured. Thanks to the stator resistance and transient time constant, the two inner current loops of the vector control scheme can be tuned. In the fifth step, the rotor time constant is determined. Next, the magnetizing inductance is measured. Note that, in this sixth step, the value of the rotor time constant is adjusted online in order to achieve $i_{sd} = i_{mr}$. Therefore, its value is verified because it is the most important parameter to obtain accurate rotor flux estimation. Thanks to the value of the rotor time constant, the flux controller of the vector control scheme can be tuned in the seventh step. Finally, the mechanical parameters of the IM coupled with the dc-machine (see below) are determined and the speed controller can be tuned.

The method based on the vector control structure has the major advantage that it can be automated. Therefore, this procedure can evaluate the motor parameters at each start-up of the experimental platform. All the results are reported in Table 1. As can be seen, very small differences are obtained between the two approaches, whatever the parameters. Therefore, one can conclude that all the IM parameters are properly determined.

Moreover, the procedure based on the vector control structure permits to determine the mechanical parameters of the IM coupled with the dc-machine. Three parameters need to be determined:

- J – the total inertia;
- T_m – the mechanical time constant;
- B – the total damping factor.

All the results are reported in Table 2.

Parameters	Conventional method	Method based on the vector control scheme
R_s	0.81 Ω	1.26 Ω
R_r	0.57 Ω	0.42 Ω
l_s	4 mH	3.9 mH
l_r	4 mH	3.9 mH
L_m	160 mH	164 mH

Table 1. IM parameters

Parameters	Values
J	0.0731 kg·m²
T_m	2.1 s
B	0.00348 kg·m²/s

Table 2. Mechanical parameters

6. Experimental results

After concluding off-line simulations using the blocks of the SimPowerSystem toolbox in Simulink software, the three control schemes are tested and compared by means of speed reference tracking, torque dynamic and flux regulation. To do so, the validated control strategies are transferred to the digital control board. Fig. 11 and 12, respectively, show the vector control algorithm implemented with Simulink and the corresponding window of the ControlDesk software which controls the dSPACE hardware. Note that more details about this work can be found in (Versèle et al., 2008; Versèle et al. 2010).
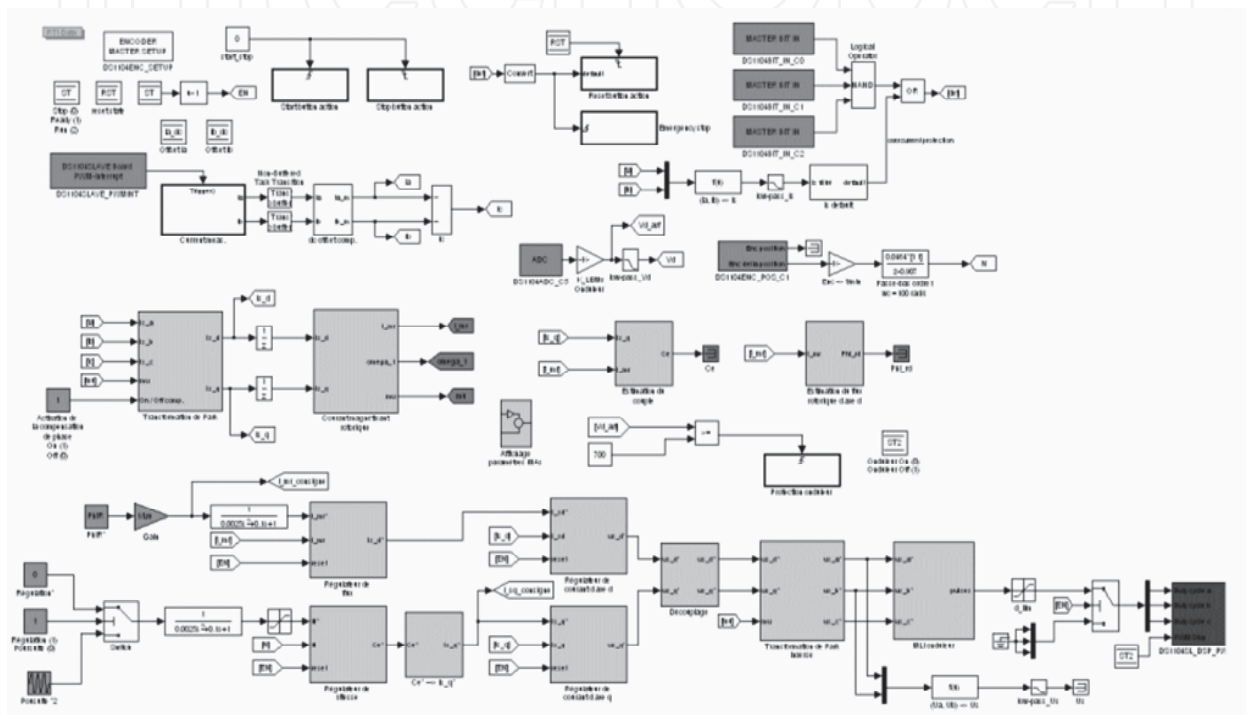
Fig. 11. Vector control algorithm implemented with Simulink

After the algorithms implementation, several tests can be carried out in order to plot the torque-speed curves in scalar control as well as to evaluate the vector control and DTC-SVM behavior in speed regulation and speed tracking. For all these tests, the switching frequency of the VSI is set at 9 kHz. The sample frequency is chosen equal to the switching frequency.

6.1 Scalar control

Fig. 13 shows the predetermined torque-speed curves (solid line) for several supplied frequencies in scalar control (in the constant flux region and in the flux-weakening region) as well as the measured torque-speed curves (circles). Note that the base frequency has been arbitrarily chosen equal to 40 Hz. It should also be noticed that, for the smaller frequencies (viz. 30 Hz, 35 Hz and 40 Hz), the measures have been stopped when instability, which can appear at low-speed and light-load operation (Kishimoto et al., 1986), is observed. One can easily conclude a very good agreement between the predetermined torque-speed curves and the measures. This confirms that the parameters are properly determined.

Fig. 14 shows the torque-speed curves in scalar control and constant rotor frequency ($s \cdot f$) operation. Note that this rotor frequency is maintained equal to 1 Hz by adjusting the slip by
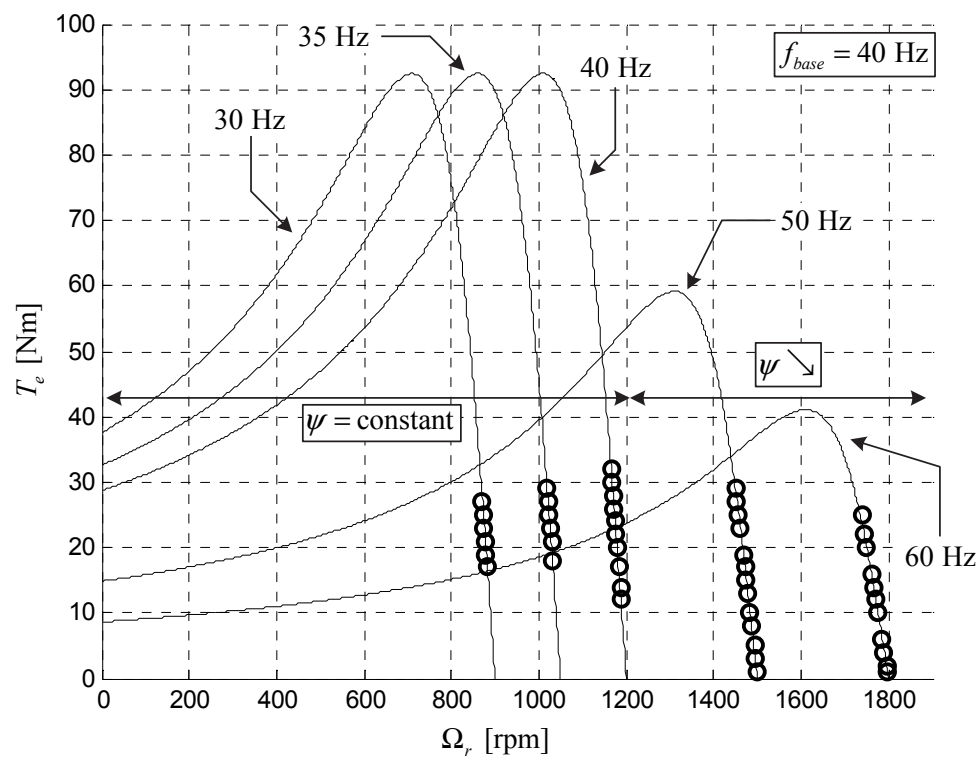
Fig. 12. ControlDesk virtual control panel

acting on the excitation of the dc-machine. Once again, one can conclude a good agreement between the predetermined curve (in solid line) and the measures performed from 30 Hz to 60 Hz (circles). Moreover, considering (3), the results can easily be explained. Indeed, in the constant flux region (below the base speed Ω_{base}), the torque is constant as the rotor frequency and the flux are constant (see (3)). Then, in the flux-weakening region, the rotor frequency remains constant but the flux decreases in inverse proportion to the frequency (and, so, to the speed). Therefore, according to (3), the torque decreases in inverse proportion to the square of the speed.

Finally, some measures have been performed in close-loop speed control with Volts/Hz control and slip regulation. Due to the slip regulation, the IM is able to rotate at the synchronous speed (900 rpm at 30 Hz and 1500 rpm at 50 Hz as $P = 2$) and, therefore, the torque-speed curves become vertical lines as shown in Fig. 15. As a final point, Fig. 16 shows a linear evolution of the torque as a function of the rotor frequency which can be explained on the basis of (3). Moreover, the slope of the regression lines, viz. 29.29 Nm/Hz at 30 Hz and 16.34 Nm/Hz at 50 Hz, are very close to the theoretical values of K_T (see (3)), viz. 28.92 Nm/Hz at 30 Hz and 16.27 Nm/Hz at 50 Hz. One can also conclude that the statistics of the regression, i.e. the R^2 and R^2_{Adj}, are very good (close to 1 and close to each other).

Fig. 13. Torque-speed curves in scalar control (solid line: predetermined curves; circles: measures)
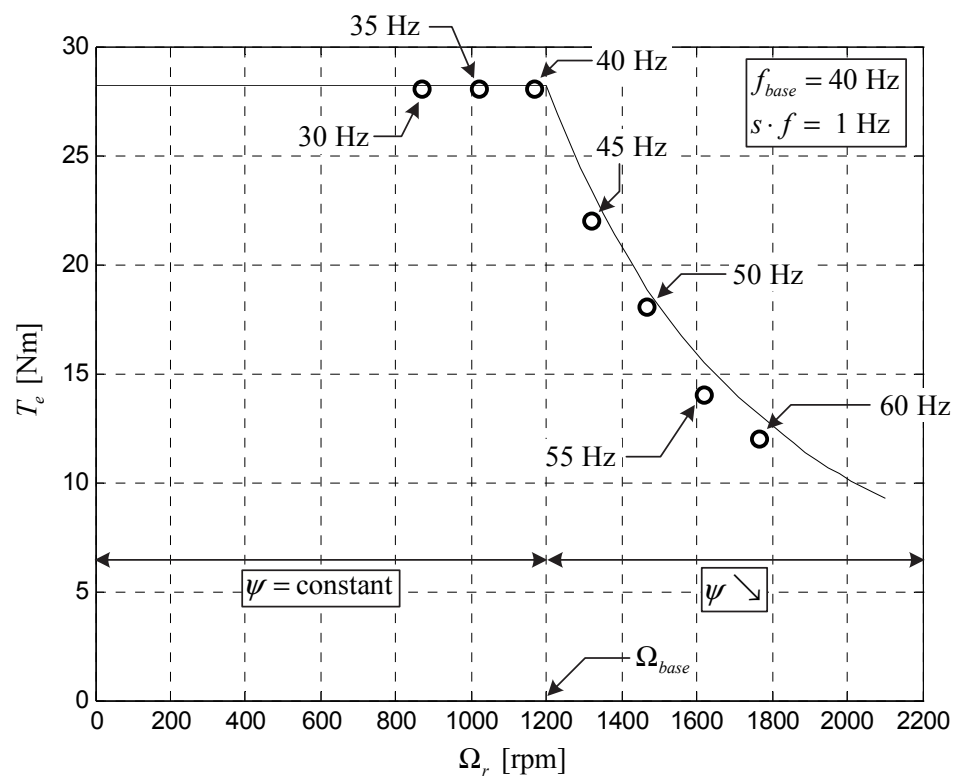
Fig. 14. Torque-speed curves in scalar control and constant rotor frequency (solid line: predetermined curves; circles: measures)
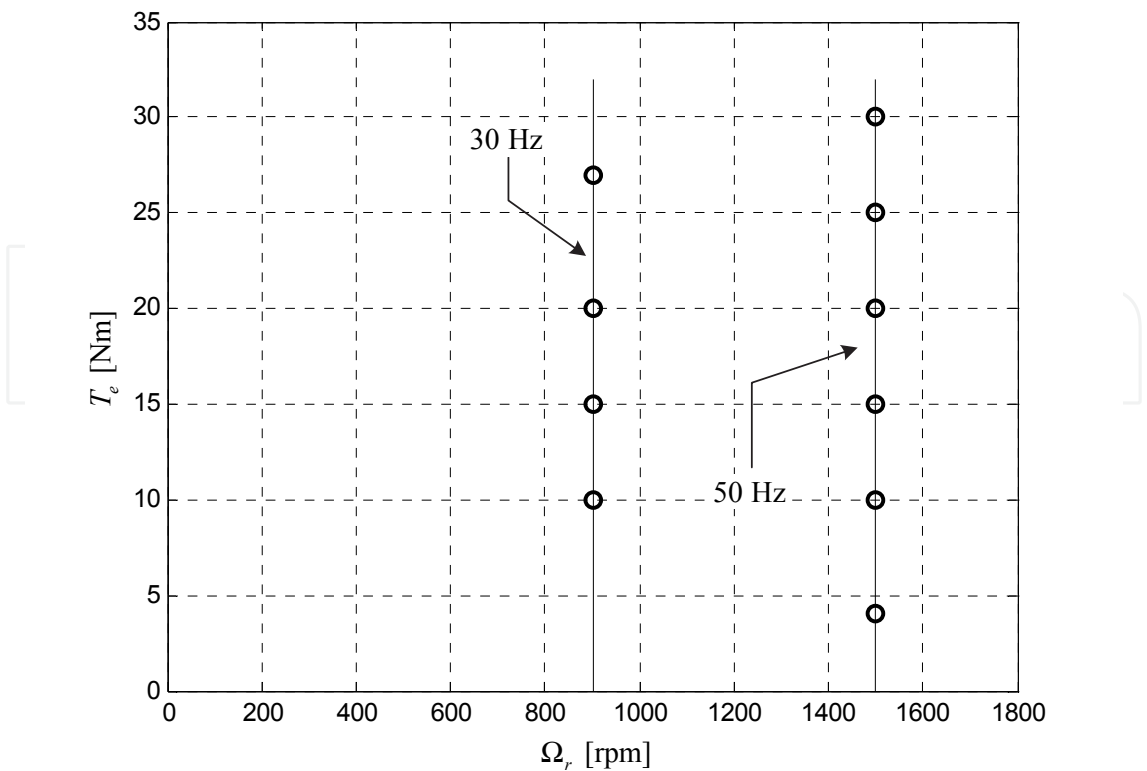
Fig. 15. Torque-speed curves in close-loop speed control with Volts/Hz control and slip regulation
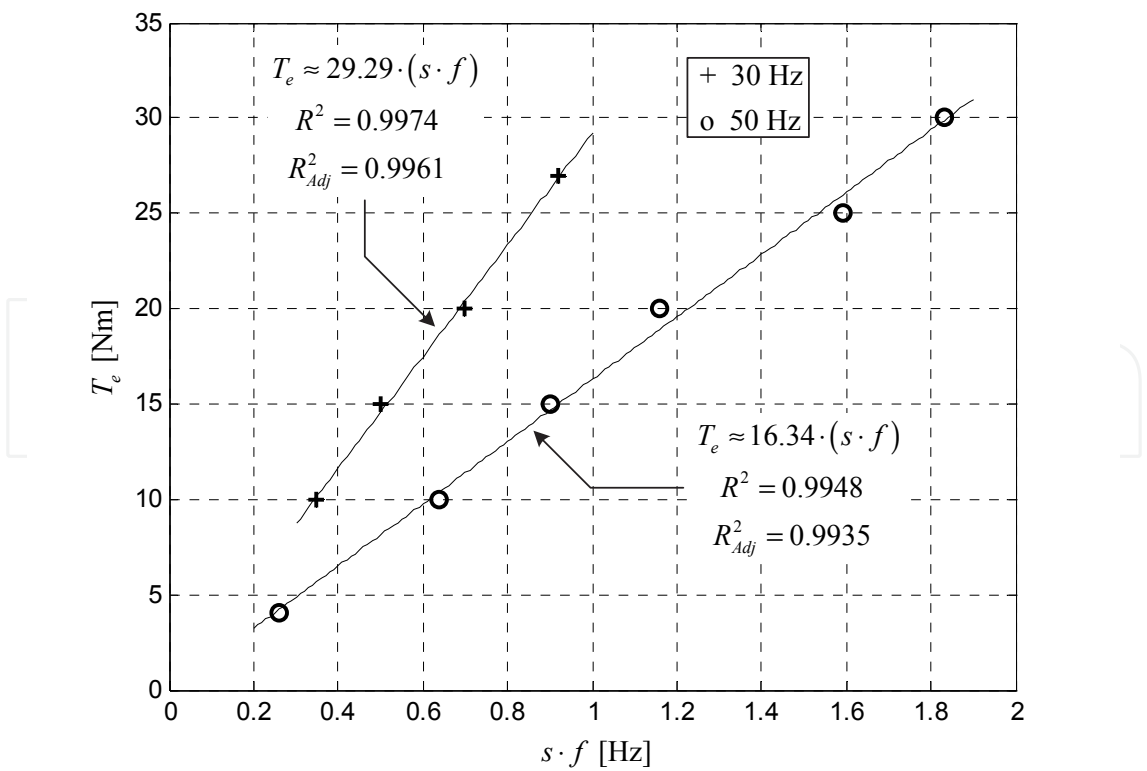

Fig. 16. Evolution of the torque as a function of the rotor frequency in close-loop speed control with Volts/Hz control and slip regulation

6.2 Vector control and DTC-SVM

In this sub-section, the results in vector control and DTC-SVM are presented and discussed. First, a speed regulation test is carried out at no-load (the load generator remains coupled to the shaft) by supplying a speed reference of 1000 rpm. In Fig. 17, the response using vector control is shown. Similarly, Fig. 18 shows the response with DTC-SVM. The speed, flux magnitude and torque are represented (from the top to the bottom). One can conclude that vector control and DTC-SVM schemes have similar dynamic responses and good speed reference tracking. One can also observe that, in vector control scheme, the rotor flux is correctly regulated and that, in DTC-SVM, the stator flux is properly regulated as well.

Then, a speed tracking test is performed at no-load. To do so, the speed reference varies from 1000 rpm to -1000 rpm as can be seen in Fig. 19 and 20. In these figures, one can observe a good response to the speed profile in vector control (Fig. 19) as well as in DTC-SVM (Fig. 20). Note that, as in the previous tests, the fluxes are correctly regulated.

In this sub-section, the two considered control schemes for IM are compared in similar operating conditions. According to the experimental results presented, one can conclude that vector control and DTC-SVM of IM drive produce comparable results in speed regulation and tracking. However, the DTC-SVM is simplest and easiest to implement than vector control. Indeed, no coordinate rotation and less PI controllers are needed. Moreover, less torque ripple is observed with DTC-SVM compare to vector control.
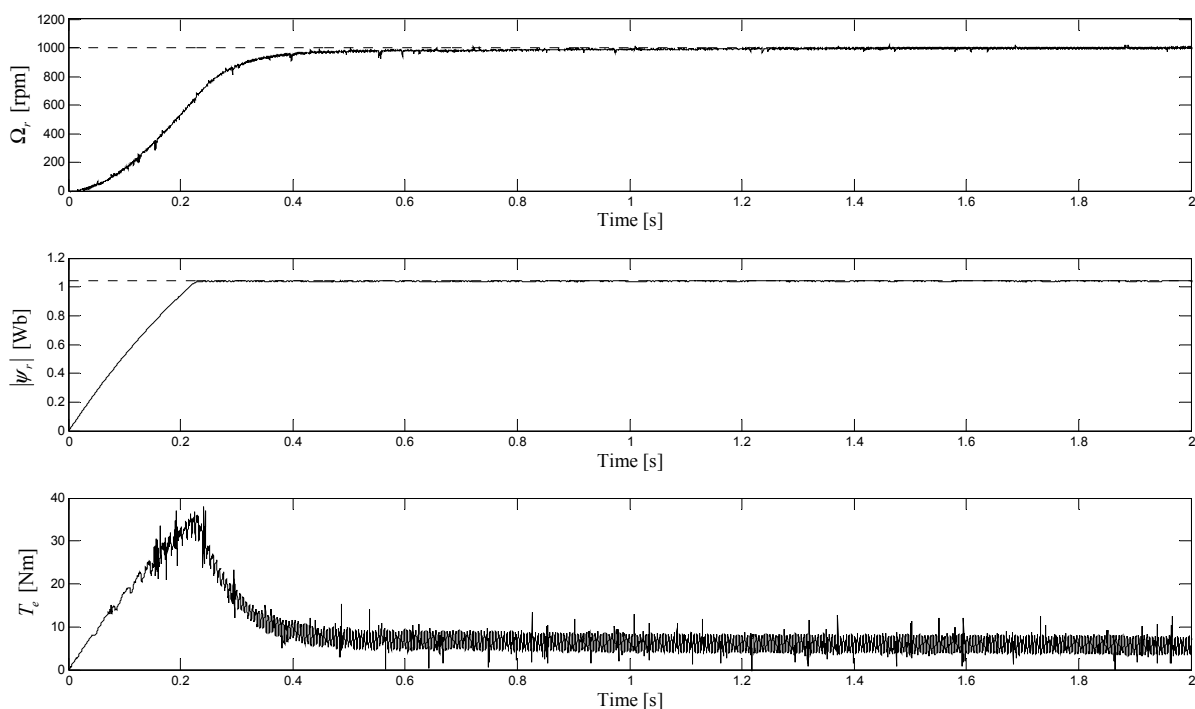

Fig. 17. Speed regulation in vector control (dotted line: speed reference; solid line: speed measured)

Finally, the effects of a load variation in vector control are shown in Fig. 21. One can conclude that such load variation does not affect the flux regulation and that, after a transient phase, the speed remains regulated at the considered speed reference (viz. 1200 rpm).
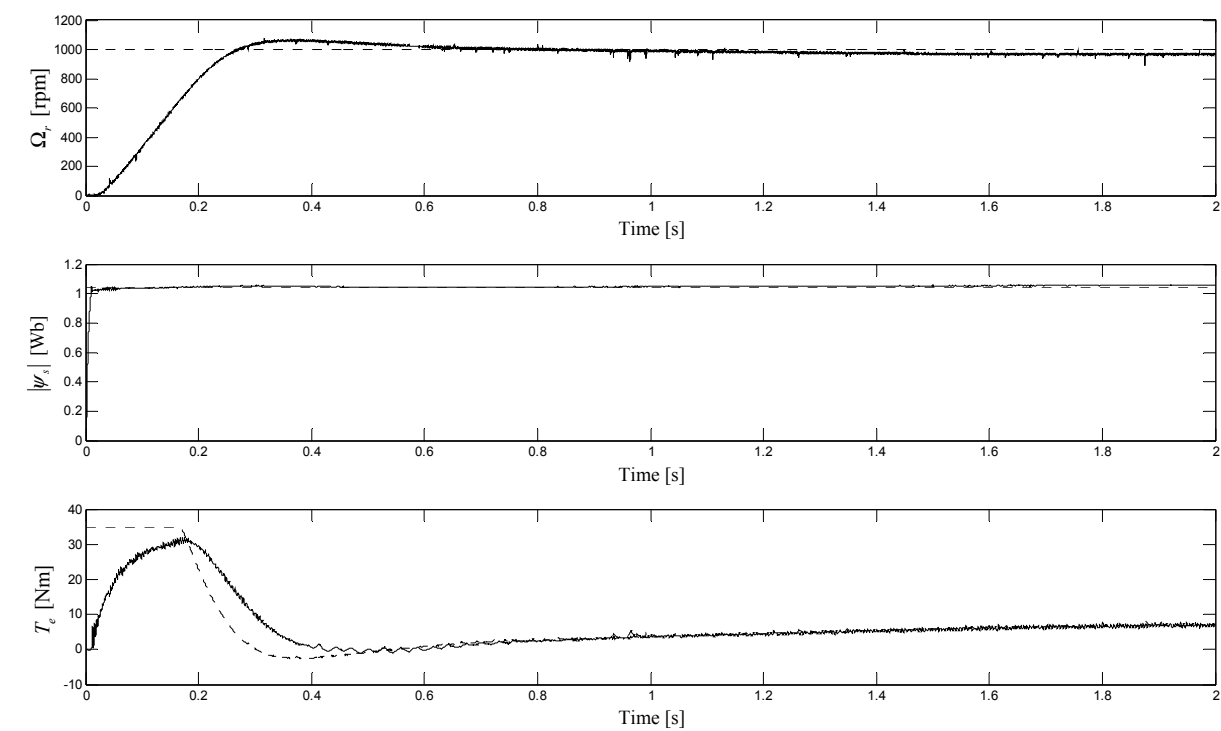
Fig. 18. Speed regulation in DTC-SVM (dotted line: speed reference; solid line: speed measured)
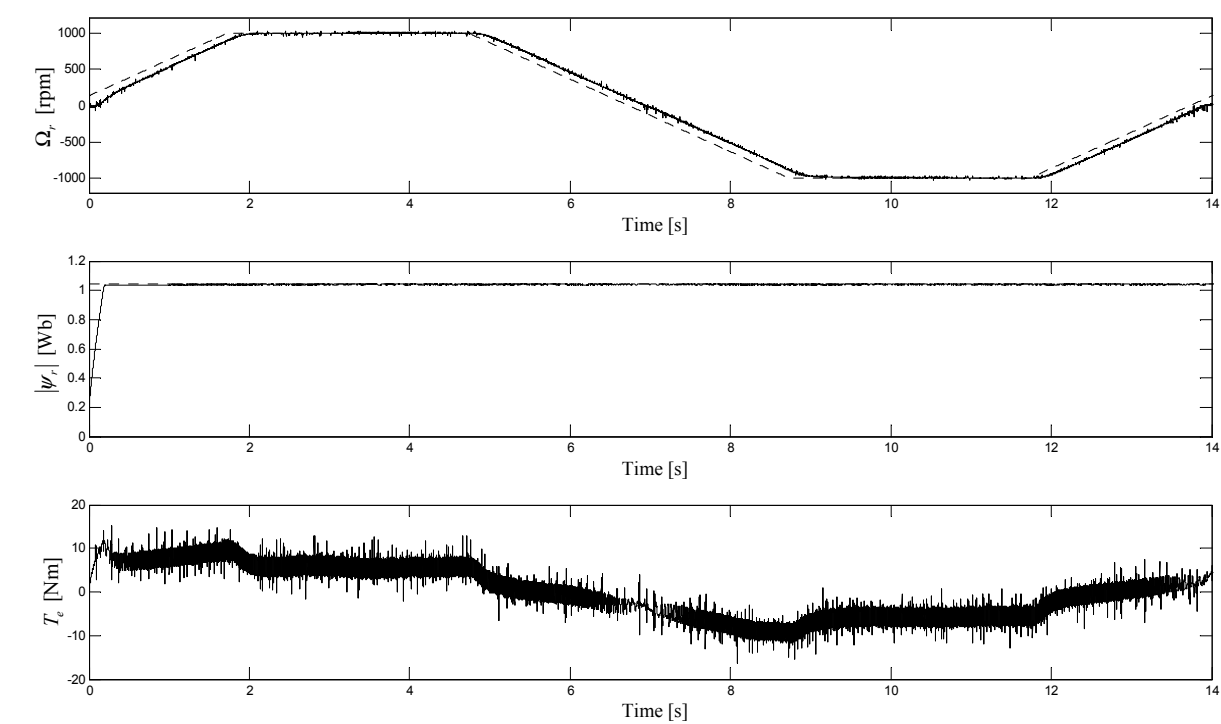

Fig. 19. Speed tracking in vector control (dotted line: speed reference; solid line: speed measured)
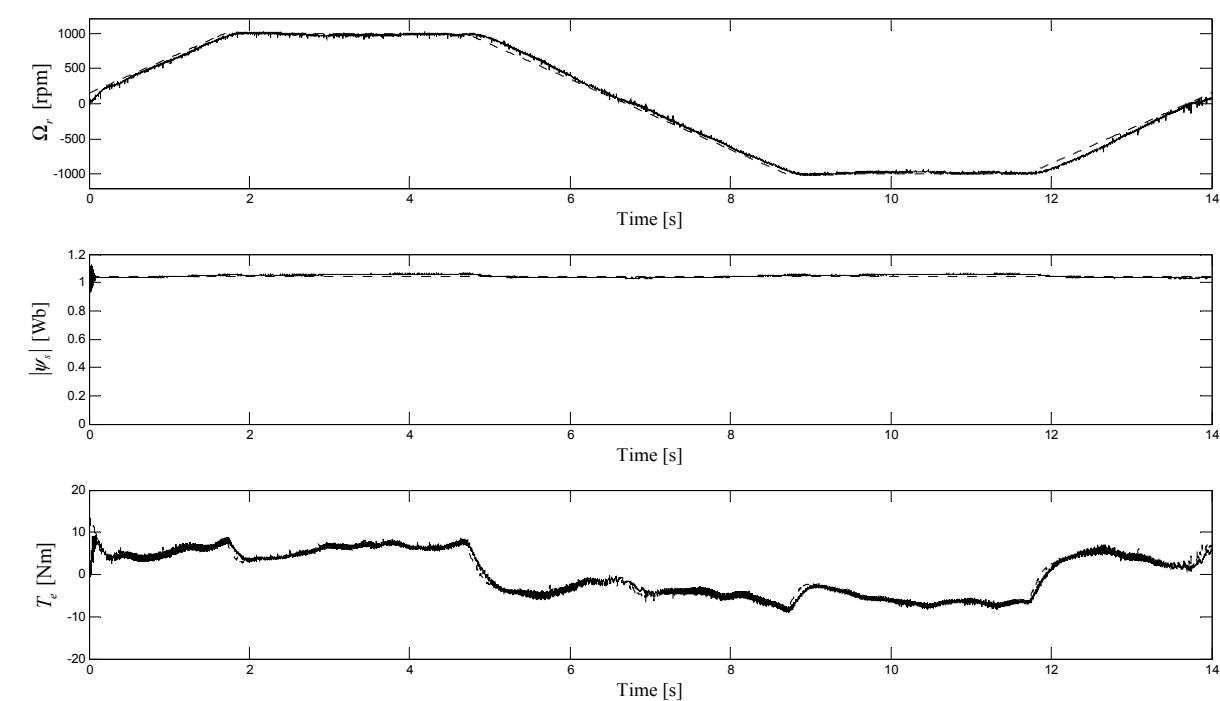
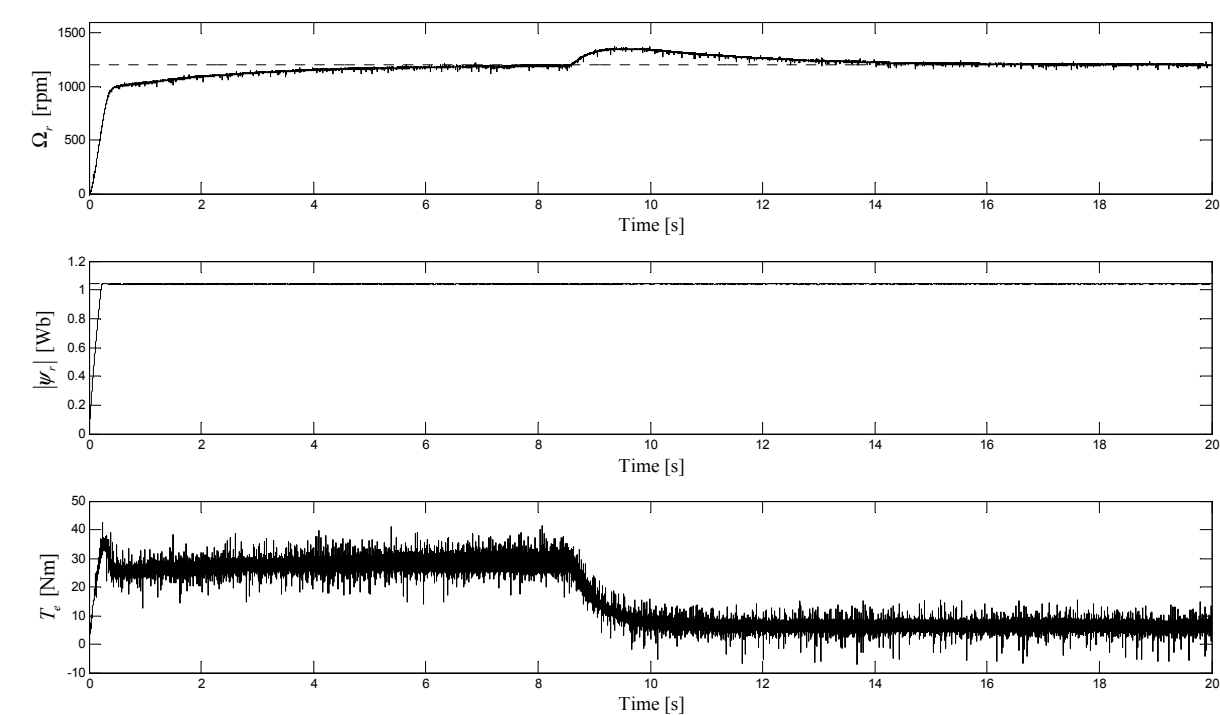Fig. 20. Speed tracking in DCT-SVM (dotted line: speed reference; solid line: speed measured)

Fig. 21. Load variation in vector control (dotted line: speed reference; solid line: speed measured)

7. Educational experience

During the lectures, students become familiar with the steady-state and dynamic models of IM and the three control schemes. Then, through the experimental setup, they are made sensitive to many aspects concerning:

- modeling and simulation using the Matlab/Simulink/dSPACE environment;
- IM parameters determination;
- IM motor drives;
- some practical aspects concerning inverters and SV-PWM.

From the students' point of view, the experimental setup presented in this chapter helps them in understanding IM parameters determination, IM steady-state as well as dynamic models and IM drives. They also found that the dSPACE platform and Matlab/Simulink environment could be used for practical teaching in other courses.

From the authors' point of view, dSPACE material offers multiple advantages from the point of education and gives a powerful tool for the teaching of IM parameters identification and drives. Moreover, thanks to this experimental setup, the students can easily put into practice a lot of theoretical knowledge.

8. Conclusion

This chapter has dealt with the implementation of three control schemes of a voltage-fed inverter IM drive, namely scalar control, vector control and DTC, using a dSPACE platform and Matlab/Simulink environment. This has been successfully integrated into "Electric Drives" course which is, usually, attended by students during their fourth year of five-year electrical engineering degree at the Faculty of Engineering (FPMs) of the University of Mons (UMons) in Belgium. It helps greatly the students in understanding the theoretical concepts taught during the lectures.

Furthermore, the dSPACE platform and Matlab/Simulink environment give a powerful tool for teaching IM parameters identification and drives. The authors are planning to use more and more this experimental system in others teaching projects.

9. References

Böcker, J. & Mathapati, S. (2007). State of the art of induction motor control, *Proceedings of 2007 International Conference on Electric Machines & Drives*, ISBN 1-4244-0743-5, Antalya, Turkey, May 2007.

Bojoi, R.; Profume, F.; Griva, G.; Teodorescu, R. & Blaabjerg, F. (2002). Advanced research and education in electrical drives by using digital real-time hardware-in-the-loop simulation, *Proceedings of the 10th International Power Electronics and Motion Control Conference*, ISBN 0-7803-7089-9, Cavtat & Dubrovnik, Croatia, September 2002.

Bose, B. K. (2002). Modern Power Electronics and AC Drives, Prentice Hall PTR, ISBN 0-13-016743-6, New Jersey, USA.

Casadei, D.; Serra, G.; Tani, A. & Zarri, L. (2005). A review on the direct torque control of induction motors, *Proceedings of the 11th International Conference on Power Electronics and Applications*, ISBN 90-75815-07-7, Dresden, Germany, September 2005.

Khambadkon, A. M. & Holtz, J. (1991). Vector-controlled induction motor drive with a self-commissioning scheme, *IEEE Transactions on Industrial Electronics*, vol. 38, no. 5, (March 1991), pp. 322-327, ISSN 0278-0046.

Kishimoto, T.; Matsumoto, K.; Kamakure, T. & Daijo, M. (1986). Stability analysis of a voltage source PWM inverter-fed induction motor drive system, *Electrical Engineering in Japan*, vol. 106, no. 6, (June 1986), pp. 32-41, ISSN 0424-7760.

Luo, G.; Liu, W.; Song, K. & Zeng, Z. (2008). dSPACE based permanent magnet motor HIL simulation and test bench, *Proceedings of the 2008 IEEE International Conference on Industrial Technology*, ISBN 978-1-4244-1706-3, Chengdu, China, April 2008.

Mäki, K.; Partanen, A.; Rauhala, T.; Repo, S. & Järventausta, P. (2005). Real-time simulation environment for power system studies using RTDS and dSPACE simulators, *Proceedings of the 11th International Conference on Power Electronics and Applications*, ISBN 90-75815-07-7, Dresden, Germany, September 2005.

Mohan, N. (2001). Advanced Electric Drives: Analysis, Control and Modeling using Simulink ®, Edition MPERE, ISBN 0-9715292-0-5, Minneapolis, USA.

Padhy, P. K. & Majhi, S. (2006). Relay based PI-PD design for stable and unstable FOPDT processes, *Computer and Chemical Engineering*, vol. 30, no. 5, (April 2006), pp. 790-796, ISSN 0098-1354.

Rodriguez, J. ; Pontt, J. ; Silva, C. ; Kouro, S. & Miranda, H. (2004). A novel direct torque scheme for induction machines with space vector modulation, *Proceedings of 35th Annual IEEE Power Electronics Specialists Conference*, ISBN 0-7803-8399-0, Aachen Germany, June 2004.

Santisteban, J. A. & Stephan, R. M. (2001). Vector control methods for induction machines: an overview, *IEEE Transactions on Education*, vol. 44, no. 2, (May 2001), pp. 170-175, ISSN 0018-9359.

Trzynadlowski, A. M.; Kazmierkowski, M. P.; Graboswski, P. Z. & Bech M. M. (1999). Three examples of DSP applications in advanced induction motor drives, *Proceedings of the 1999 American Control Conference*, ISBN 0-7803-4990-3, San Diego, USA, June 1999.

Versèle, C.; Deblecker, O. & Lobry, J. (2008). Implementation of a vector control scheme using dSPACE material for teaching induction motor drives and parameters identification, *Proceedings of the 2008 International Conference on Electrical Machines*, ISBN 978-1-4244-1736-0, Vilamoura, Portugal, September 2008.

Versèle, C.; Deblecker, O. & Lobry, J. (2010). Implementation of advanced control schemes using dSPACE material for teaching induction motor drive, *International Journal of Electrical Engineering Education*, vol. 47, no. 2, (April 2010), pp. 151-167, ISSN 0020-7209.

MATLAB for Engineers - Applications in Control, Electrical Engineering, IT and Robotics

Edited by Dr. Karel Perutka

The book presents several approaches in the key areas of practice for which the MATLAB software package was used. Topics covered include applications for: -Motors -Power systems -Robots -Vehicles The rapid development of technology impacts all areas. Authors of the book chapters, who are experts in their field, present interesting solutions of their work. The book will familiarize the readers with the solutions and enable the readers to enlarge them by their own research. It will be of great interest to control and electrical engineers and students in the fields of research the book covers.

How to reference

In order to correctly reference this scholarly work, feel free to copy and paste the following:

Christophe Versèle, Olivier Deblecker and Jacques Lobry (2011). Implementation of Induction Motor Drive Control Schemes in MATLAB/Simulink/dSPACE Environment for Educational Purpose, MATLAB for Engineers - Applications in Control, Electrical Engineering, IT and Robotics, Dr. Karel Perutka (Ed.), ISBN: 978-953-307-914-1, InTech, Available from: http://www.intechopen.com/books/matlab-for-engineers-applications-in-control-electrical-engineering-it-and-robotics/implementation-of-induction-motor-drive-control-schemes-in-matlab-simulink-dspace-environment-for-ed

INTECH

open science | open minds